Progress In Electromagnetics Research, Vol. 129, 33–49, 2012

MODELING OF OPTICAL TRAPPING USING DOUBLE NEGATIVE INDEX FISHNET METAMATERIALS

T. Cao[1, *] and M. J. Cryan[2]

[1]Department of Biomedical Engineering, Faculty of Electronic information and Electrical Engineering, Dalian University of Technology, China

[2]Department of Electrical and Electronic Engineering, University of Bristol, Bristol, UK

Abstract—We calculate the optical forces exerted on nanoparticles in close proximity to the surface of fishnet metamaterials based on metal/dielectric/metal films when irradiated at near infrared wavelength. These forces show resonant frequencies similar to the magnetic resonant frequencies in the double negative index fishnet metamaterial. We also show that the optical force can be enhanced by optimizing the geometry of the fishnet to provide a stronger magnetic resonant dipole. In contrast to most other plasmonic nanostructure which always obtaining trapping force using an electrical resonant dipole, our presented structure utilizes the magnetic resonance to provide a trapping force. We have found that it is suitable for optical trapping of nanoscale particles at illumination intensities of just $1\,\mathrm{mW}/\mu\mathrm{m}^2$ and the force is sufficient to overcome gravity.

1. INTRODUCTION

The gradient of the light field has been used to generate optical force to trap micrometer-sized particles, a configuration known as "optical tweezers" [1]. This strong gradient force that confines the objects in three dimensions has been exploited in dielectric nanostructures, leading to many exciting applications in colloid dynamics [2], particle sorting [3], lab-on-a-chip technology [4], optical trapping and transport of biomolecules [5, 6]. However, in conventional optical tweezers, light usually has a repelling force on the particles due to the focused gradient beam [7–10]. In a recent study, researchers have shown

Received 3 May 2012, Accepted 4 June 2012, Scheduled 13 June 2012

* Corresponding author: Tun Cao (caotun1806@dlut.edu.cn).

that the trapping force can also be obtained using a gradientless light beam [11]. But the highest achievable intensity gradient is bounded by the diffraction of the light beam, which limits the maximum optical trapping force for a given input power, recently surface plasmon (SP) based systems have been proposed to address the problem [12–14]. In SP devices, the collective optical excitation of electrons along a metal dielectric interface confines the electromagnetic waves to deep subwavelength scale [15, 16]. The optical field strength and trapping force will be then significantly enhanced by the strong optical confinement.

Recently, researchers have exploited the trapping force for the various plasmonic nanostructures, for example, gold nanoparticle dimers [17], all-optical actuation of nanomechanical systems [18] and negative refractive index metamaterials [19–21]. Compared to conventional optical tweezers, plasmonic nanostructures can create high local field enhancements and provide an optical force to be more suitable for trapping nanoparticles [22–25]. Lately, an array of Au bowtie nanoantennas (BNAs) was demonstrated for optical trapping and manipulation of the submicrometer sized objects when illuminated by laser radiation [26]. These periodic plasmonic structures have a strong electrical resonance because each unit cell functions as an electrical quadrupole. When the laser frequency is chosen close to the electrical resonance of BNAs, a much stronger optical force can be achieved due to the large localized intensities close to the surface. To our knowledge, most plasmonic nanostructures discussed above typically rely on the excitation of the electrically resonant dipole, but the optical trapping force exerted on the nanoparticles induced by magnetic dipole resonance has not been reported yet.

In recent years, researchers have found that a pronounced magnetic dipole resonance can be excited in metamaterials [27, 28]. A well known application of this magnetic resonance is in achieving double negative index by using multilayer metamaterials [29–48]. In this article, we want to explore the optical trapping forces in such a multilayer fishnet metamaterial. Unlike single plasmonic layer metamaterials where $\lambda \gg L$, in which λ is the resonant wavelength and L is the lattice constant of the metamaterial, this multilayer fishnet metamaterial can achieve a double negative index in both near-infrared and visible region on the condition that $L > \frac{\lambda}{4}$ [30, 49].

We have found that the resonance of the optical forces is very close to the resonance of the magnetic dipole excited by the fishnet metamaterial when illuminated in the near infrared. The effect of the fishnet's geometry (round and elliptical holes) on the strength of the forces has also been investigated. It has been shown that structure

formed from an elliptical nanohole array (ENA) possesses a greater value of trapping force than a circular nanohole array (CNA) due to its stronger magnetic dipole resonance. We have also shown that the optical force is sufficient to overcome gravity at illumination intensities of just $1\,\mathrm{mW}/\mu\mathrm{m}^2$.

2. METHOD

In this section, we discuss the method for computing the optical force on the dielectric particle near the surface of MDM fishnet metamaterials. We firstly use the three dimensional finite difference time domain method (3D FDTD) to solve Maxwell's equations for the scattering problem of an incident plane wave illuminating the fishnet metamaterial. After obtaining the field profile of the structure, we integrate the stress tensor over the surface of the nanoparticle in the simulation domain to calculate the optical force on the particle [50]:

$$\vec{F} = \oiint_S \left(\hat{n} \cdot \overleftrightarrow{\sigma}^{opt}\right) dS \tag{1}$$

where

$$\overleftrightarrow{\sigma}_{ij}^{opt} = \varepsilon E_i E_j^* + \mu H_i H_j^* - \frac{1}{2}\delta_{ij}\left(\varepsilon |E|^2 + \mu |H|^2\right) \tag{2}$$

is the Maxwell stress tensor, S is a bounding surface around the nanoparticle. Here E and H are the electric and magnetic fields, ε and μ are the relative permittivity and permeability. δ_{ij} is the Kronecker delta. The total optical force $\vec{F}$ (assuming Casimir and heating effects to be negligible) consists of an electromagnetic radiation pressure $\overrightarrow{F_{rad}}$ and a near field electromagnetic force $\overrightarrow{F_{nr}}$ induced by the MDM fishnet metamaterial, where $\overrightarrow{F_{rad}}$ depends on the spectrum of the coefficients of the structure according to the Equation (3)

$$\overrightarrow{F_{rad}} = \frac{(2R + A)P}{c} \tag{3}$$

where R is reflection, A is absorption, P is the power of the incident light and c is the speed of the light in vacuum [51]. As shown in Figure 1(a), $\overrightarrow{F_{rad}}$ acting on the dielectric particle is an upward pushing force and $\overrightarrow{F_{nr}}$ is a downward dragging force. When the light is trapped and strongly absorbed by fishnet metamaterial for example $A = 1$, we can obtain the minimum value of $\overrightarrow{F_{rad}} = \frac{p}{c}$ therefore the maximum value of $\overrightarrow{F_{nr}}$ to trap the particle. All fields are well defined and the integration can be straightforwardly carrier out with 3D EM Explorer Studio (a 3D FDTD commercial software).

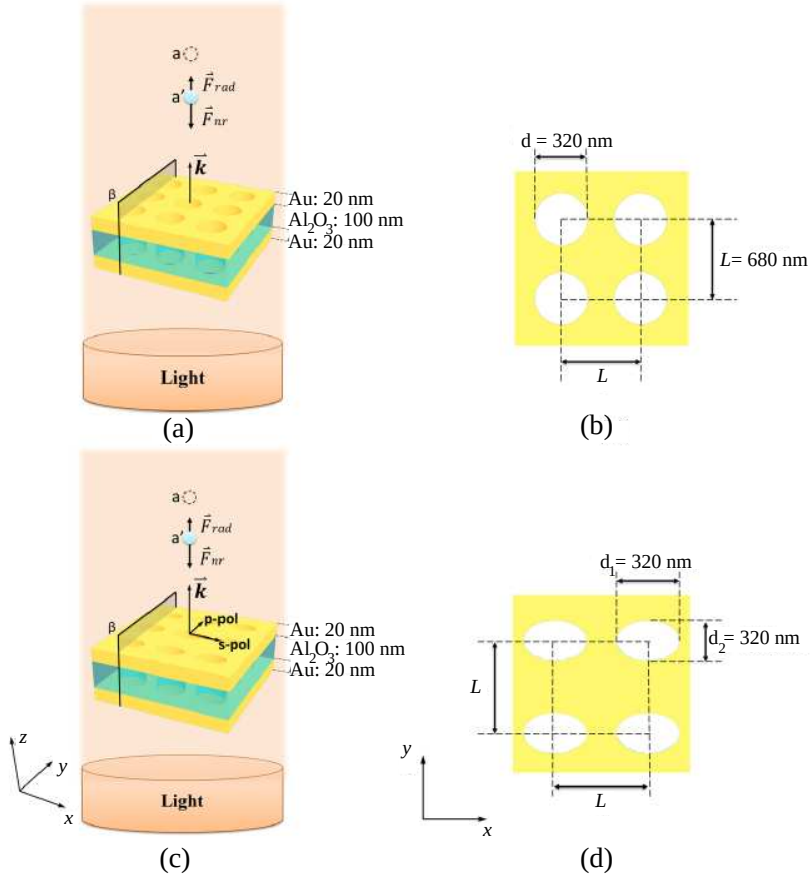

Figure 1. (a) Schematic of a MDM fishnet metamaterials consisting of an Al_2O_3 dielectric layer between two Au films perforated with a square array of round holes suspended in air. The lattice constant is $L = 680\,\text{nm}$ and hole diameters are $d = 320\,\text{nm}$. (b) Illustration of the square lattice of a circular nanohole array (CNA). (c) Schematic of a MDM fishnet metamaterials consisting of a Al_2O_3 dielectric layer between two Au films perforated with a square array of elliptical holes suspended in the air. The lattice constant is $L = 680\,\text{nm}$ and hole diameters are $d_1 = 320\,\text{nm}$ and $d_2 = 280\,\text{nm}$. (d) Illustration of the square lattice of an elliptical nanohole array (ENA).

3. SIMULATION RESULTS AND DISCUSSION

We begin our study with an analysis of a two-dimensional (2D) square periodic array of round and elliptical holes penetrating through

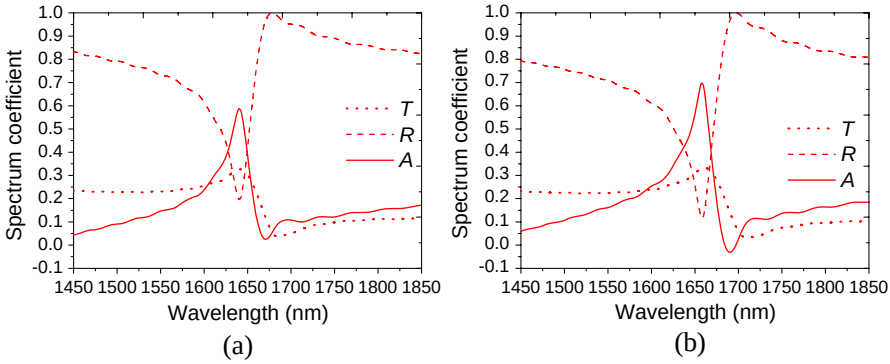

Figure 2. (a) Spectral coefficients of the MDM fishnet metamaterial with CNA. (b) Spectral coefficient of the MDM fishnet metamaterial with ENA.

the structure which consists of two-metallic films (20 nm thick Au) separated by a dielectric layer (100 nm thick Al_2O_3), the unit cells are periodically extended along x and y direction and the lattice axes coincide with the coordinate axes, where lattice constant: $L = 680$ nm, the round hole diameter is: d =320 nm, and elliptical hole diameters are: d_1 =320 nm and $d_2 = 280$ nm. Schematic representations of these structures are shown in Figure 1.

As noted above, this paper uses a commercial 3D FDTD solution to study the structure. A simple Drude model is used for the dielectric constant of Au, $\varepsilon(\omega) = 1 - \frac{\omega_p^2}{[\omega(\omega+i\omega_c)]}$, where $\omega_p = 1.37 \times 10^{16}\,\mathrm{s}^{-1}$ is the plasma frequency and $\omega_c = 2.04 \times 10^{14}\,\mathrm{s}^{-1}$ is the collision frequency for bulk Au [30]. The refractive index of Al_2O_3 is 1.62. The computational domain has perfectly match layer (PML) absorbing boundaries in the z direction and periodic boundaries in the x-y plane. The FDTD mesh size is 2 nm to provide an accurate calculation on the plasmonic effect. We illuminate the structure with round holes by an upward plane wave with the E field along the x axis as described in Figure 1(a). A p polarized plane wave source was used to illuminate the structure with elliptical holes due to its asymmetric as shown in Figure 1(c), where p polarization is defined by the incident electric field vector parallel to the short axis of the elliptical holes. Both of the structures are illuminated in the near infrared regime with power density of $1\,\mathrm{mW}/\mu\mathrm{m}^2$. The power intensity is chosen to be readily tolerated by the thin Au films and creates sufficient optical force to exceed the gravitational force.

We firstly compute the spectrum of CNA in Figure 2(a). It shows that little transmission signal can be detected around the wavelength

of 1640 nm. Simultaneously, a reflection dip and absorption peak can also be achieved. These are most likely determined by the magnetic resonance which results from a pair of finite-width Au films separated by a dielectric layer along the direction of the incident light. We show the spectrum of the ENA in Figure 2(b). At the resonant wavelength of 1658 nm, it is found that ENA possesses a deeper reflectance dip and higher absorption peak than the CNA. This is due to the fact that the thinner metallic strip width along the short axis of the elliptical aperture can be used to improve the impedance matching between the air and the metamaterial [31].

The so-called material parameters, effective permittivity ε_{eff} and effective permeability μ_{eff} of the MDM fishnet metamaterials are extracted using the well-known Nicholson-Ross-Weir (NRW) method [52, 53]. The normalized characteristic impedance and refractive index of the structure at normal incidence angle are found from the Fresnel-Airy formulas [54]:

$$\eta = \sqrt{\frac{(1+R)^2 - T^2}{(1-R)^2 - T^2}} \tag{4}$$

$$n = \frac{1}{kD}\left[\arccos\left[\frac{1-R^2+T^2}{2T}\right] + 2\pi m\right] \tag{5}$$

and the effective material parameters are expressed as

$$\varepsilon_{eff} = n/\eta, \quad \mu_{eff} = n\eta \tag{6}$$

Here, n is refractive index, η is impedance, D is the thickness of the structure, $k = \omega/c$, c is the speed of light, and m is an arbitrary integer. The signs of n and η and the value of m are commonly chosen as described in [55].

Using the procedure described in Section 2, we calculated $\vec{F}$ on a dielectric particle which is 180 nm above the surface of the structures as shown in Figure 1. We assume that the particle has a relative dielectric permittivity $\varepsilon_p = 2.25$ and the radius of the particle is $R_p = 80$ nm. In Figure 3(a), it can be seen that the dispersion of $\vec{F}$ has a local minimum at the wavelengths of 1640 nm and 1658 nm for the CNA and ENA respectively, corresponding to the absorption peaks shown in Figure 2. Figure 3(a) shows that $\vec{F}$ in the ENA at 1658 nm is stronger than CNA at 1640 nm. It is believed that the greater value of $\vec{F}$ in ENA is a consequence of the structure's higher absorption induced by the stronger magnetic dipole resonance.

This can be explained based on the calculation of the permeability of the structures. As shown in Figure 3(b), the ENA gives rise to a more negative value of real part of the permeability ($\mathrm{Re}(\mu_{eff})$) than the

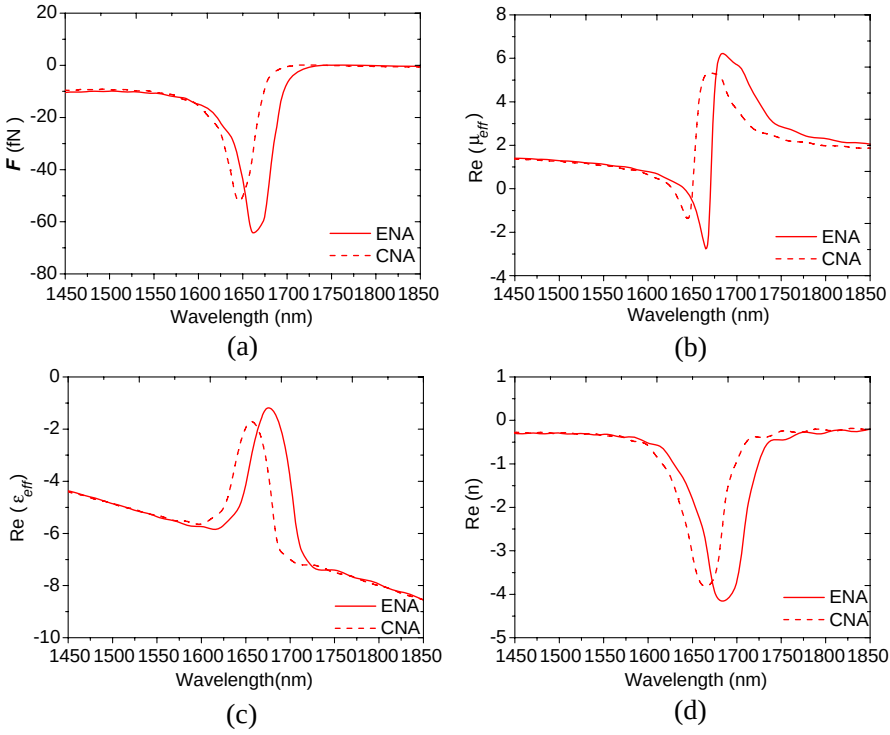

Figure 3. (a) Comparison of $\vec{F}$ acting on the nanoparticles ($R_p = 80\,\text{nm}$ and $\varepsilon_p = 2.25$), 180 nm above the MDM fishnet metamaterials between CNA and ENA when illuminated under an incident field of $1\,\text{mW}/\mu\text{m}^2$. (b) Comparison of the real part of the permeability ($\text{Re}(\mu_{eff})$) between the ENA and CNA. (c) Comparison of the real part of the permittivity $\text{Re}(\varepsilon_{eff})$ between the ENA and CNA. (d) Comparison of the real part of refractive index $\text{Re}(n)$ between the ENA and CNA.

CNA. The less negative $\text{Re}(\mu_{eff})$ of the CNA mainly originates from a weaker magnetic resonance owing to a poor impedance match between the metamaterial and the surrounding medium [31]. Particularly, we observe that the resonance wavelengths of the $\text{Re}(\mu_{eff})$ are close to the resonance wavelengths of $\vec{F}$ where the dielectric particle can obtain the maximum trapping force $\vec{F}$ shown in Figure 3(a). We can then understand that magnetic dipole resonance in MDM fishnet metamaterials will also contribute to the optical trapping force. The value of $\vec{F}$ is associated with the strength of the magnetic dipole

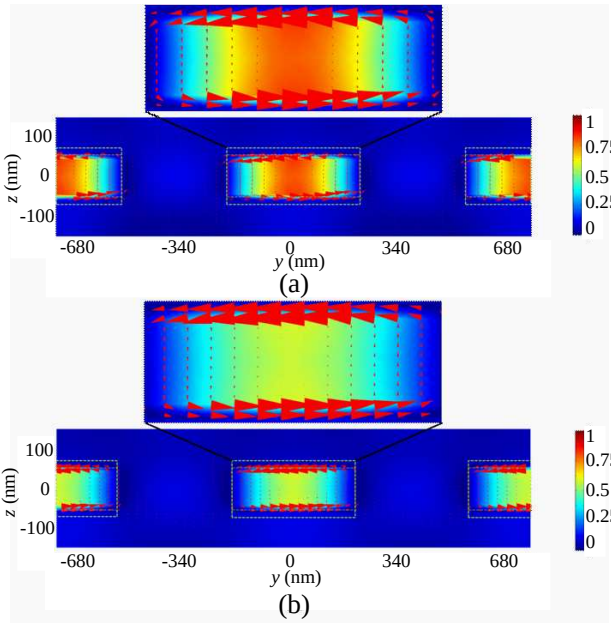

Figure 4. (a) A map of the normalized magnetic field intensity distribution at 1658 nm resonance wavelength for a cross section along the β plane (z-x plane) in the ENA, a zoom in picture has been presented in the top inset. (b) A map of the normalized magnetic field intensity distribution at 1640 nm resonance wavelength for a cross section along the β plane (z-x plane) in the CNA a zoom in picture has been presented in the top inset.

resonance: a more negative $\mathrm{Re}(\mu_{eff})$ or stronger magnetic dipole will result in a greater value of $\vec{F}$. In Figures 3(c) and (d), we have also simulated $\mathrm{Re}(\varepsilon_{eff})$ and $\mathrm{Re}(n)$ for the ENA and CNA. As shown in Figure 3(c), $\mathrm{Re}(\varepsilon_{eff})$ is negative over an overlapping frequency range with the negative $\mathrm{Re}\,(\mu_{eff})$ in both the ENA and CNA. In Figure 3(d), it can be seen that $\mathrm{Re}(n)$ of the ENA shows a more negative dip near the resonance frequency owing to the stronger permeability resonance shown in Figure 3(b).

To better understand this feature, Figure 4 shows the magnetic field distributions at the magnetic resonant wavelengths 1658 nm and 1640 nm for the ENA and CNA respectively at a β plane shown in Figure 1. In the field maps of Figure 4, the arrows show the electric displacement current whereas the colour shows the magnitude of the magnetic field. The formation of closed displacement current loops

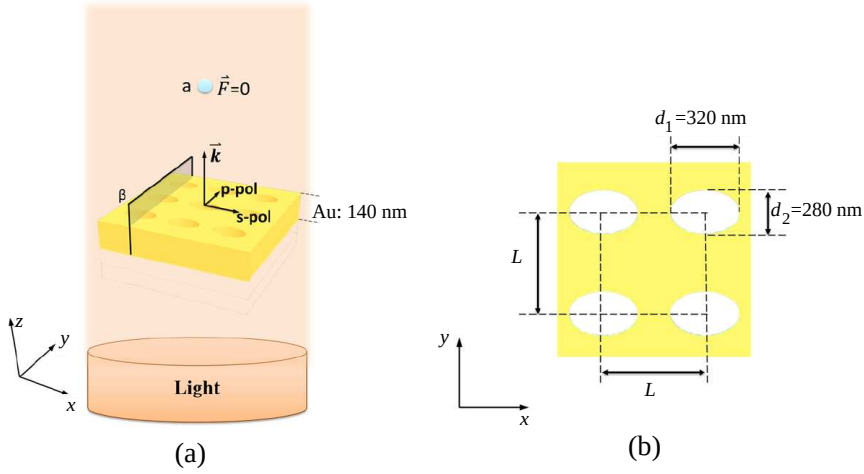

Figure 5. (a) schematic of ENA embedded through a single Au layer. The lattice constant is $L = 680\,\text{nm}$ and hole diameters are $d_1 = 320\,\text{nm}$ and $d_2 = 280\,\text{nm}$. (b) Illustration of the square lattice of ENA.

can be observed. According to Faraday's law, magnetic dipolar modes are excited at these magnetic resonant wavelengths. Therefore, the magnetic field can be efficiently confined between the two Au layers to support a magnetic resonance at which light is trapped and strongly absorbed to create a higher value of the magnetic dipolar optical force [56]. In particular, the localized magnetic fields in the ENA are enhanced more strongly than in the CNA, implying that a greater value of magnetic dipolar force could be obtained. It is interesting to compare the gravitational force on the particle with the optical trapping force. The gravitational force on a 80 nm radius nanoparticle is around 0.02 fN which is four orders smaller than $\vec{F}$ under $1\,\text{mW}/\mu\text{m}^2$ illumination intensity. So the optical forces discussed here are easy to distinguish and the magnetic dipolar force will be big enough to manipulate a nanoparticle against gravity. It is also found that the magnetic dipolar force depends on wavelength, hence providing dynamic controllability and spectral selectivity.

In order to further justify the fact that $\vec{F}$ is mainly induced by the magnetic resonant dipole, we have simulated the identical lateral structure, however, with a single Au layer as shown in Figure 5. In Figure 6(a), we show the displacement current in the β plane. We note that the electric displacement current does not form a loop and hence, the magnetic field cannot be efficiently confined in the single Au layer to support a magnetic resonance. We then calculated $\text{Re}(\mu_{eff})$ of the

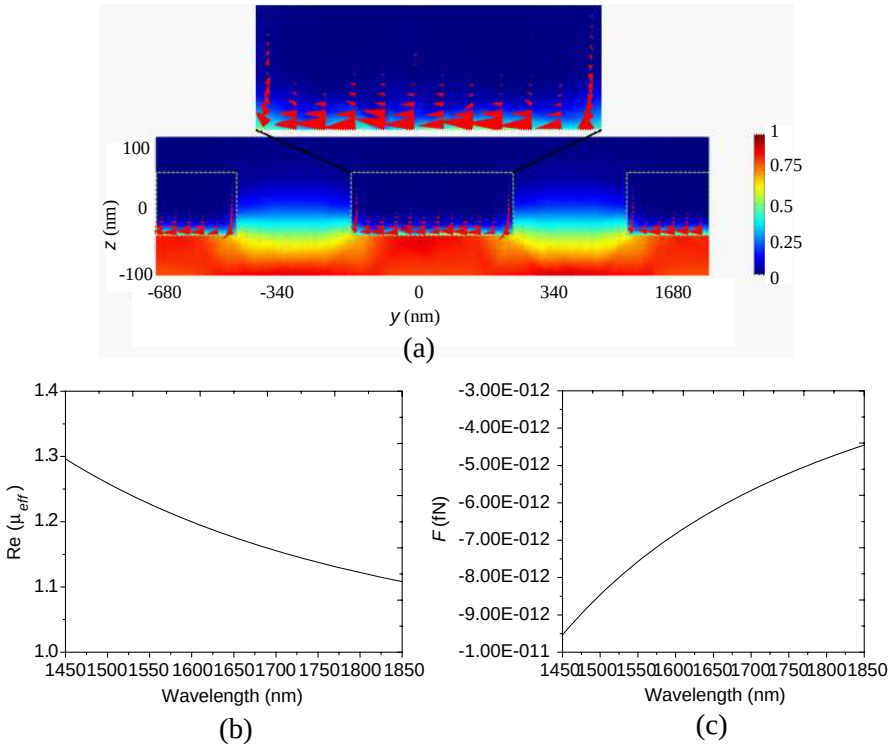

Figure 6. (a) A map of the normalized magnetic field intensity distribution for a cross section along the β plane (z-x plane) in ENA perforating through a single Au layer, a zoom in picture has been presented in the top inset. (b) The real part of the permeability ($\mathrm{Re}(\mu_{eff})$) of ENA perforating through a single Au layer. (c) $\vec{F}$ acting on the nanoparticles ($R_p = 80\,\mathrm{nm}$ and $\varepsilon_p = 2.25$), 180 nm above the single Au layer ENA when illuminated under an incident field of $1\,\mathrm{mW}/\mu\mathrm{m}^2$.

structure shown in Figure 6(b) and in agreement with the displacement map, the ENA embedded through the single Au layer does not possess a negative $\mathrm{Re}(\mu_{eff})$. In Figure 6(c), $\vec{F}$ on the same dielectric particle which is 180 nm above the surface of the structure is shown and a zero value of $\vec{F}$ is observed. This suggests that the optical trapping force in multilayer fishnet metamaterial is mainly due to the magnetic resonant dipole.

In this section, we analyze $\vec{F}$ for lossy particles, which are 180 nm above the surface of the structures, by introducing the loss term δ into

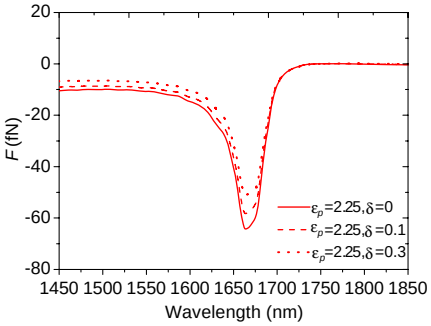

Figure 7. $\vec{F}$ exerted on the nanoparticle 180 nm above ENA for lossy particles $\varepsilon = \varepsilon_p + i\delta$ with $R_p = 80\,\text{nm}$

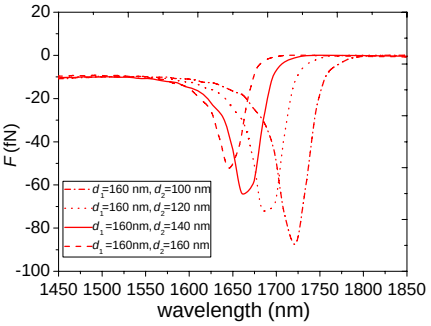

Figure 8. $\vec{F}$ acting on the nanoparticles ($R_p = 80\,\text{nm}$ and $\varepsilon_p = 2.25$), 180 nm above the MDM fishnet metamaterials at different value of d_1, d_2 as shown in the inset.

permittivity $\varepsilon = \varepsilon_p + i\delta$. We choose two different values for the loss term: $\delta = 0.1$ and $\delta = 0.3$. In Figure 7, we present the comparison of $\vec{F}$ acting on a nanoparticles ($R_p = 80\,\text{nm}$, $\varepsilon_p = 2.25$) with and without loss. It is shown that the waveform of $\vec{F}$ is similar in both cases, but the optical trapping force reduces when loss increases. This can be explained by the fact that the momentum transfer from the photons to the nanopaticles creates additional pushing forces as the result of non-elastic interactions [11].

Figure 8 shows the total optical force $\vec{F}$ at different ratios of the diameters of the elliptical hole ($\frac{d_1}{d_2}$) with the same lattice constant: $L = 680\,\text{nm}$. It is shown that the absolute value of $\vec{F}$ increases as the ratio of the diameters increases from 1 to 1.6. It is most likely due to the fact that as the ratio increases from unity, the more anisotropy will be introduced to the unit cell of the ENA, so $\vec{F}$ becomes stronger. It is also shown that the $\vec{F}$curve redshifts when the ratio of the diameters increases.

4. CONCLUSION

In conclusion, we have demonstrated the possibility of realizing optical trapping force using double negative index fishnet metamaterials in the near infrared regime. It has been shown that an ENA exhibits a greater value of optical trapping force $\vec{F}$ than a CNA. The mechanism of this enhanced optical force is explained based on both magnetic

dipole resonance and magnetic field distributions in the negative index structures. The optical trapping force induced by the magnetic dipole resonance enables the applications of optical tweezers at the nanometer scale, opening a new realm for optical trapping and manipulation of nanoparticles such as biomolecules and quantum dots.

ACKNOWLEDGMENT

We acknowledge the financial support from National Natural Science Foundation of China (Grant No. 61172059 and 61071123), Ph.D. Programs Foundation of Ministry of Education of China (Grant No. 20110041120015), Postdoctoral Gathering Project of Liaoning Province (Grant No. 2011921008), and The Fundamental Research for the Central University (Grant No. DUT12JB01).

REFERENCES

1. Ashkin, A., J. M. Dziedzic, J. E. Bjorkholm, and S. Chu, "Observation of a single-beam gradient force optical trap for dielectric particles," *Optics Letters*, Vol. 11, No. 5, 288–290, 1986.
2. Roichman, Y., B. Sun, A. Stolarski, and D. G. Grier, "Influence of nonconservative optical forces on the dynamics of optically trapped colloidal spheres: The fountain of probability," *Physical Review Letters*, Vol. 101, No. 12, 128301(1–4), 2008.
3. MacDonald, M. P., G. C. Spalding, and K. Dholakia, "Microfluidic sorting in an optical lattice," *Nature*, Vol. 426, 421–424, 2003.
4. Eriksson, E., J. Enger, B. Nordlander, N. Erjavec, K. Ramser, M. Goksor, S. Hohmann, T. Nystrom, and D. Hanstorp, "A microfluidic system in combination with optical tweezers for analyzing rapid and reversible cytological alterations in single cells upon environmental changes," *Lab on a Chip*, Vol. 7, 71–76, 2007.
5. Yang, A. H. J., S. D. Moore, B. S. Schmidt, M. Klug, M. Lipson, and D. Erickson, "Optical manipulation of nanoparticles and biomolecules in sub-wavelength slot waveguides," *Nature*, Vol. 457, 71–75, 2009.
6. Mandal, S., X. Serey, and D. Eickson, "Nanomanipulation using silicon photonic crystal resonators," *Nano Letters*, Vol. 10, 99–104, 2010.
7. Roichman, Y., B. Sun, Y. Roichman, J. Amato-Grill, and D. G. Grier, "Optical forces arising from phase gradients," *Physical Review Letters*, Vol. 100, No. 1, 013602(1–4), 2008.

8. Karásek,V., T. Cizmár, O. Brzobohatý, P. Zemánek, V. Garcés-Chávez, and K. Dholakia, "Long-range one-dimensional longitudinal optical binding," *Physical Review Letters*, Vol. 101, No. 14, 143601(1–4), 2008.
9. Albaladejo, S., M. I. Marqués, M. Laroche, and J. J. Sáenz, "Scattering forces from the curl of the spin angular momentum of a light field," *Physical Review Letters*, Vol. 102, No. 11, 113602(1–4), 2009.
10. Ng, J., Z. F. Lin, and C. T. Chan, "Theory of optical trapping by an optical vortex beam," *Physical Review Letters*, Vol. 104, No. 10, 103601(1–4), 2010.
11. Novitsky, A., C. W. Qiu, and H. F. Wang, "Single gradientless light beam drags particles as tractor beams," *Physical Review Letters*, Vol. 107, No. 20, 203601(1–4), 2011.
12. Novotny, L., R. X. Bian, and X. S. Xie, "Theory of nanometric optical tweezers," *Physical Review Letters*, Vol. 79, No. 4, 645–648, 1997.
13. Quidant, R., D. Petrov, and G. Badenes, "Radiation forces on a Rayleigh dielectric sphere in a patterned optical near field," *Optics Letters*, Vol. 30, No. 9, 1009–1011, 2005.
14. Xu, H. and M. Kall, "Surface-plasmon-enhanced optical forces in silver nanoaggregates," *Physical Review Letters*, Vol. 89, No. 24, 246802(1–4), 2002.
15. Ishikawa, A., S. Zhang, D. A. Genov, G. Bartal, and X. Zhang, "Deep subwavelength terahertz waveguides using gap magnetic plasmon," *Physical Review Letters*, Vol. 102, No. 4, 043904(1–4), 2009.
16. Choi, H., D. F. P. Pile, S. Nam, G. Bartal, and X. Zhang, "Compressing surface plasmons for nano-scale optical focusing," *Optics Express*, Vol. 17, No. 9, 7519–7524, 2009.
17. Nome, R. A., M. J. Guffey, N. F. Scherer, and S. K. Gray, "Plasmonic interactions and optical forces between au bipyramidal nanoparticle dimers," *The Journal of Physical Chemistry A*, Vol. 113, No. 16, 4408–4415, 2009.
18. Woolf, D., M. Loncar, and F. Capasso, "The forces from coupled surface plasmon polaritons in planar waveguides," *Optics Express*, Vol. 17, No. 22, 19996–20011, 2009.
19. Ambrosio, L. A. and H. E. Hernández-Figueroa, "Fundamentals of negative refractive index optical trapping: Forces and radiation pressures exerted by focused Gaussian beams using the generalized Lorenz-Mie theory," *Biomedical Optics Express*, Vol. 1, 1284–1301,

2010.

20. Ambrosio, L. A. and H. E. Hernández-Figueroa, "Radiation pressure cross sections and optical forces over negative refractive index spherical particles by ordinary bessel beams," *Applied Optics*, Vol. 50, 4489–4498, 2011.
21. Ambrosio, L. A. and H. E. Hernández-Figueroa, "Spin angular momentum transfer from plane waves and azimuthally symmetric focused beams to negative refractive index spherical particles," *Biomedical Optics Express*, Vol. 2, 2354–2363, 2011.
22. Ploschner, M., M. Mazilu, T. F. Krauss, and K. Dholakia, "Optical forces near a nanoantenna," *Journal of Nanophotonics*, Vol. 4, 041570(1–13), 2010.
23. Grigorenko, A. N., N. W. Roberts, M. R. Dickinson, and Y. Zhang, "Nanometric optical tweezers based on nanostructured substrates," *Nature Photonics*, Vol. 2, 365–370, 2008.
24. Righini, M., P. Ghenuche, S. Cherukulappurath, V. Myroshnychenko, F. J. Garcia de Abajo, and R. Quidant, "Nano-optical trapping of rayleigh particles and escherichia coli bacteria with resonant optical antennas," *Nano Letters*, Vol. 9, No. 10, 3387–3391, 2009.
25. Tsuboi, Y., T. Shoji, N. Kitamura, M. Takase, K. Murakoshi, Y. Mizumoto, and H. Ishihara, "Optical trapping of quantum dots based on gap-mode-excitation of localized surface plasmon," *The Journal of Physical Chemistry Letters*, Vol. 1, No. 15, 2327–2333, 2010.
26. Roxworthy, B. J., K. D. Ko, A. Kumar, K. H. Fung, E. K. C. Chow, G. L. Liu, N. X. Fang, and K. C. Toussaint, "Application of plasmonic bowtie nanoantenna arrays for optical trapping, stacking, and sorting," *Nano Letters*, Vol. 12, No. 2, 796–801, 2012.
27. Chen, H., L. Ran, J. Huangfu, X. M. Zhang, K. Chen, T. M. Grzegorczyk, and J. A. Kong, "Magnetic properties of S-shaped split-ring resonators," *Progress In Electromagnetics Research*, Vol. 51, 231–247, 2005.
28. Chen, H. S., L. Huang, and X. X. Cheng, "Magnetic properties of metamaterial composed of closed rings," *Progress In Electromagnetics Research*, Vol. 115, 317–326, 2011.
29. Zhang, S., W. Fan, K. J. Malloy, S. R. Brueck, N. C. Panoiu, and R. M. Osgood, "Near-infrared double negative metamaterials," *Optics Express*, Vol. 13, No. 13, 4922–4930, 2005.
30. Zhang, S., W. Fan, N. C. Panoiu, K. J. Malloy, R. M. Osgood,

and S. R. J. Brueck, "Experimental demonstration of near-infrared negative-index metamaterials," *Physical Review Letters*, Vol. 95, No. 13, 137404(1–4), 2005.

31. Zhang, S., W. Fan, N. C. Panoiu, K. J. Malloy, R. M. Osgood, and S. R. J. Brueck, "Demonstration of metal-dielectric negative-index metamaterials with improved performance at optical frequencies," *Journal of the Optical Society of America B*, Vol. 23, No. 3, 434–438, 2006.
32. Menzel, C., C. Rockstuhl, T. Paul, F. Lederer, and T. Pertsch, "Retrieving effective parameters for metamaterials at oblique incidence," *Physical Review B,* Vol. 77, 195328(1–8), 2008.
33. Ourir, A., R. Abdeddaim, and J. de Rosny, "Tunable trapped mode in symmetric resonator designed for metamaterials," *Progress In Electromagnetics Research*, Vol. 101, 115–123, 2010.
34. Oraizi, H., A. Abdolali, and N. Vaseghi, "Application of double zero metamaterials as radar absorbing materials for the reduction of radar cross section," *Progress In Electromagnetics Research*, Vol. 101, 323–337, 2010.
35. Duan, Z., Y. Wang, X. Mao, W.-X. Wang, and M. Chen, "Experimental demonstration of double-negative metamaterials partially filled in a circular waveguide," *Progress In Electromagnetics Research*, Vol. 121, 215–224, 2011.
36. Feng, T., Y. Li, H. Jiang, W. Li, F. Yang, X. Dong, and H. Chen, "Tunable single-negative metamaterials based on microstrip transmission line with varactor diodes loading," *Progress In Electromagnetics Research*, Vol. 120, 35–50, 2011.
37. Xu, S., L. Yang, L. Huang, and H. Chen, "Experimental measurement method to determine the permittivity of extra thin materials using resonant metamaterials, *Progress In Electromagnetics Research*, Vol. 120, 327–337, 2011.
38. Shao, J., H. Zhang, Y. Lin, and H. Xin, "Dual-frequency electromagnetic cloaks enabled by Lc-based metamaterial circuits," *Progress In Electromagnetics Research*, Vol. 119, 225–237, 2011.
39. Zhou, H., F. Ding, Y. Jin, and S. He, "Terahertz metamaterial modulators based on absorption," *Progress In Electromagnetics Research*, Vol. 119, 449–460, 2011.
40. Navarro-Cia, M., V. Torres Landivar, M. Beruete, and M. Sorolla Ayza, "A slow light fishnet-like absorber in the millimeter-wave range," *Progress In Electromagnetics Research*, Vol. 118, 287–301, 2011.
41. Araujo, M. G., J. M. Taboada, J. Rivero, and F. Obelleiro,

"Comparison of surface integral equations for left-handed materials," *Progress In Electromagnetics Research*, Vol. 118, 425-440, 2011.

42. Giamalaki, M. I. and I. S. Karanasiou, "Enhancement of a microwave radiometry imaging system's performance using left handed materials," *Progress In Electromagnetics Research*, Vol. 117, 253–265, 2011.
43. Li, J., F.-Q. Yang, and J. Dong, "Design and simulation of L-shaped chiral negative refractive index structure," *Progress In Electromagnetics Research*, Vol. 116, 395–408, 2011.
44. Canto, J. R., C. R. Paiva, and A. M. Barbosa, "Dispersion and losses in surface waveguides containing double negative or chiral metamaterials," *Progress In Electromagnetics Research*, Vol. 116, 409–423, 2011.
45. Liu, S.-H. and L.-X. Guo, "Negative refraction in an anisotropic metamaterial with a rotation angle between the principal axis and the planar interface," *Progress In Electromagnetics Research*, Vol. 115, 243–257, 2011.
46. Huang, L. and H. Chen, "Multi-band and polarization insensitive metamaterial absorber," *Progress In Electromagnetics Research*, Vol. 113, 103–110, 2011.
47. Li, M., H.-L. Yang, X.-W. Hou, Y. Tian, and D.-Y. Hou, "Perfect metamaterial absorber with dual bands," *Progress In Electromagnetics Research*, Vol. 108, 37–49, 2010.
48. Choi, J. and C. Seo, "High-efficiency wireless energy transmission using magnetic resonance based on negative refractive index metamaterial," *Progress In Electromagnetics Research*, Vol. 106, 33–47, 2010.
49. García-Meca, C., J. Hurtado, J. Martí, A. Martínez, W. Dickson, and A. V. Zayats, "Low-loss multilayered metamaterial exhibiting a negative index of refraction at visible wavelengths," *Physical Review Letters*, Vol. 106, No. 6, 067402(1–4), 2011.
50. Zhao, R., P. Tassin, T. Koschny, and C. M. Soukoulis, "Optical forces in nanowire pairs and metamaterials," *Optics Express*, Vol. 18, No. 25, 25665–25676, 2010.
51. Zhang, J., K. F. MacDonald, and N. I. Zheludev, "Optical gecko toe: Optically controlled attractive near-field forces between plasmonic metamaterials and dielectric or metal surfaces," *Physical Review B*, Vol. 85, No. 20, 205123(1–5), 2012.
52. Ziolkowski, R. W., "Design, fabrication, and testing of double negative metamaterials," *IEEE Transactions on Antennas and*

Propagation, Vol. 51, No. 7, 1516–1529, 2003.

53. Nicolson, A. M. and G. F. Ross, "Measurement of the intrinsic properties of materials by time-domain techniques," *IEEE Transactions on Instrumentation and Measurement*, Vol. 19, No. 4, 377–382, 1970.
54. Simovski, C. R., "Bloch material parameters of magnetodielectric metamaterials and the concept of Bloch lattices," *Metamaterials*, Vol. 1, 62–80, 2007.
55. Smith, D. R., S. Schultz, P. Markos, and C. M. Soukoulis, "Determination of effective permittivity and permeability of metamaterials from reflection and transmission coefficients," *Physical Review B*, Vol. 65, No. 19, 195104(1–5), 2002.
56. Hao, J., L. Zhou, and M. Qiu, "Nearly total absorption of light and heat generation by plasmonic metamaterials," *Physical Review B*, Vol. 83, No. 16, 165107(1–12), 2011.